

## Proposed Post-doc Subject

FMJH/LMH

Mathématiques du Calcul Scientifique et de l'Ingénierie

### Jing-Rebecca Li

INRIA Saclay, Equipe IDEFIX, UMA, ENSTA Paris  
828, Boulevard des Maréchaux, 91762 Palaiseau, France  
[jingrebecca.li@inria.fr](mailto:jingrebecca.li@inria.fr)

## Fourier representation of the diffusion MRI signal using layer potentials

**1. Introduction.** Diffusion magnetic resonance imaging (diffusion MRI) is a promising non-invasive imaging modality that can probe the tissue microstructure by encoding the motion of water molecules with magnetic gradient pulses [32, 13]. The goal of various imaging protocols is often the recovery of some biological parameters of interest, such as axon diameter and density [38, 30], dendrite structure [11, 29], effective diffusion coefficient [3]. However, in the past, researchers sometimes could not fully validate some of these proposed protocols due to the lack of ground truth. Therefore, recent works have started to include numerical simulations as a part of the validation process [28, 34].

Concerning the current numerical simulation methods for diffusion MRI applications, two popular groups of approaches are Monte-Carlo methods and Bloch-Torrey PDE-based methods. Monte-Carlo methods use random walkers to mimic the diffusion process in a geometrical configuration. The Bloch Torrey PDE-based methods solve the Bloch-Torrey partial differential equation, which describes the evolution of the complex transverse water proton magnetization under the influence of diffusion-encoding magnetic field gradient pulses. The predominant numerical methods to solve this PDE include the finite difference method [14], the finite element method [17, 21, 2], and the Matrix Formalism method [6, 7, 18]. In addition to numerical efficiency, some Bloch-Torrey PDE-based methods allow for a better understanding of the diffusion mechanism. Our previous works in Bloch-Torrey PDE-based neuron simulations demonstrate that diffusion MRI signals reflect the cellular organization of cortical gray matter, and these signals are sensitive to cell size and the presence of large neurons such as the spindle (von Economo) neurons [33, 36, 19, 5].

The Matrix Formalism method [6, 7], which decomposes the solution of the Bloch-Torrey PDE onto a Laplacian eigenbasis, provides another interesting perspective to the diffusion MRI signal. One can address many fundamental theoretical questions about the diffusion MRI signal thanks to the eigendecomposition. In some ways, the Matrix Formalism method inspired us to decompose the diffusion MRI signal into a Fourier type basis. Contrary to the Laplacian eigenbasis, the Fourier basis functions themselves do not depend on the geometrical confinement. This independence should allow for the comparison between various geometries and provides a new spectral perspective.

Based on potential theory from classical mathematics, we propose a new method that provides a Fourier type representation of the diffusion MRI signal. The main challenge to overcome involves the fundamental solution of the diffusion equation, also

known as the heat kernel, which has a singularity in time. In theory, infinite Fourier modes are required to represent the heat kernel due to the singularity, while only finite Fourier modes are accessible for practical computation. This practical limitation may lead to the Gibbs phenomenon that could degrade the approximation accuracy [35]. In order to overcome this challenge, we follow the path of several previous works [8, 15, 16, 9] focusing on the evaluation of heat potentials. In particular, in [8], the authors proposed several fundamental ideas, such as 1) splitting the heat potential into a local in time part and a history part in order to overcome the singularity of the heat kernel; 2) approximating the local in time part by asymptotics; 3) leveraging the exponential decay of the history part to represent it using a few Fourier modes. These ideas are crucial to the Fourier type representation of the diffusion MRI signal that we derive in this paper.

Despite the intrinsic similarity between thermal conduction and diffusion process, in the literature, there have not been previous works about the representation of the diffusion MRI signal via potential theory, and certainly not by using a Fourier basis for layer potentials. As a first step in addressing this subject, we restrict ourselves to the 2D diffusion MRI setting with impermeable interfaces. We also restrict ourselves to simplified conditions on the diffusion-encoding gradient, specifically, we derive our method under the narrow pulse assumption, where the diffusion-encoding pulse duration is very short compared to the delay between the pulses. These two assumptions allow us to apply the theory developed for the diffusion kernel to the diffusion MRI application.

The main steps of our method are 1) transforming the Bloch-Torrey PDE to the diffusion equation using the narrow pulse assumption on the diffusion-encoding sequence; 2) formulating the solution of the diffusion equation using the single layer potential; 3) approximating the singular part of the single layer potential using an asymptotic expansion and solving the integral equation; 4) storing the non-singular part of the single layer potential using the Fourier coefficients, leveraging the fast decay in the spectrum; 5) computing the diffusion MRI signal using the above representation. We call our method the Fourier Potential Method (FPM).

**2. Post-doc project.** Here we present FPM simulation results on two realistic axons. The microscopy image (Figure 1) and the axon sections are obtained using the AxonDeepSeg segmentation framework [37]. With these irregular shapes, analytical solutions are not accessible, so we computed the reference signals by finite element simulations using the SpinDoctor toolbox [17]. We show, in Figure 2, the dMRI signals in 40 directions as well as the relative errors. Our method agrees with the finite element reference signals. For the middle b-value ( $4ms/\mu m^2$ ), the relative error is less than 5%. One should note that the magnetization of the two adjacent axons is computed simultaneously by sharing the same Fourier basis. This feature is different from the Matrix Formalism method, which requires geometry-dependent bases.

One of the main features of our method is the availability of the spectrum of the smooth part of the magnetization field. The projection to the Fourier basis functions provides a unified spectrum space for different geometries. Since our method provides a Fourier like representation of the diffusion MRI signal, this can potentially facilitate new physical and biological signal interpretation in the future.

The goal of the post-doc project is to study the Fourier representation of 2D geometrical objects coming from the brain white matter. We are interested in relating the properties of the Fourier coefficients to geometrical parameters such as the size and shape of axons.

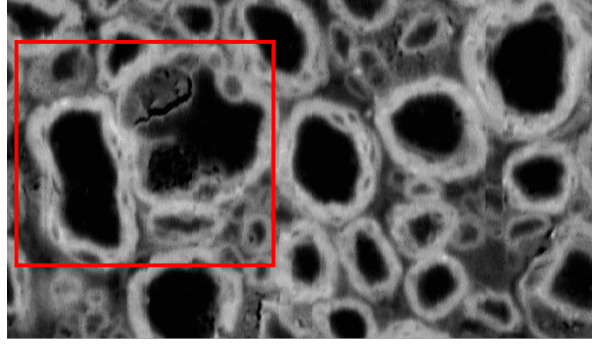


FIG. 1. The microscopy image of axons from AxonDeepSeg. Two adjacent axons are selected.

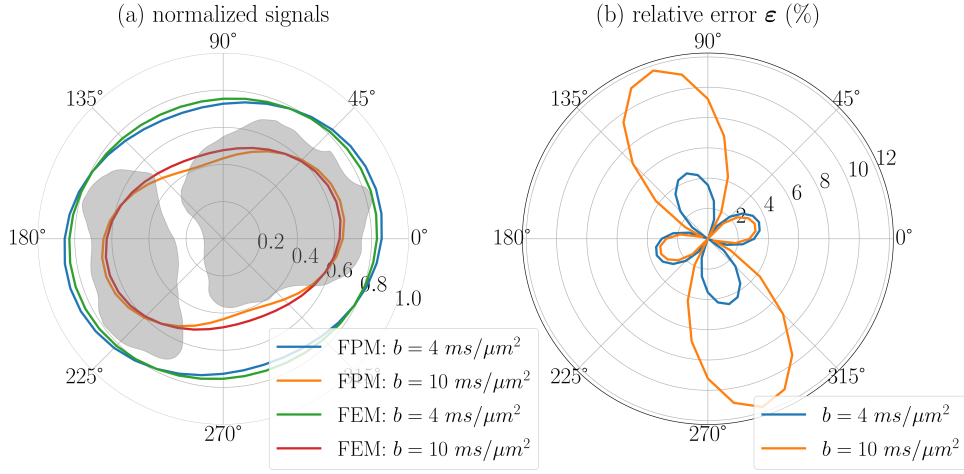


FIG. 2. Comparison of FPM with FEM. (a) the normalized signals simulated by FPM and FEM. The gray areas illustrate the shapes of the two adjacent axons. The physical parameters are:  $\mathcal{D}_0 = 2 \times 10^{-3} \mu\text{m}^2/\mu\text{s}$ ,  $\delta = 2 \text{ ms}$ ,  $\Delta = 100 \text{ ms}$ . The discretization parameters of the FPM are:  $\eta = 50 \mu\text{s}$ ,  $\nu_{\max} = 2 \mu\text{m}^{-1}$ ,  $\Delta\nu = 0.05 \mu\text{m}^{-1}$ ,  $\Delta x = 0.01 \mu\text{m}$ , and  $\Delta t = 50 \mu\text{s}$ . The signals are simulated in 40 directions evenly distributed on a unit circle. (b) the relative errors in percent.

## Mathematical background

**3. Mathematical frame of diffusion MRI.** Suppose one would like to simulate the diffusion MRI signal due to spins inside a biological cell and assume that the spin exchange across the cell membrane is negligible under the simulation conditions. Let  $\Omega$  be the domain that describes the geometry of the biological cell and let  $\Gamma = \partial\Omega$  be the cell membrane.

**3.1. Bloch-Torrey PDE.** In diffusion MRI, a time-varying magnetic field gradient is applied to the tissue to encode water diffusion. Denoting the effective time profile of the diffusion-encoding magnetic field gradient by  $f(t)$ , and let the vector  $\mathbf{g}$  contain the amplitude and direction information of the magnetic field gradient, the complex transverse water proton magnetization in the rotating frame satisfies the Bloch-Torrey PDE:

$$(3.1) \quad \frac{\partial}{\partial t} M(\mathbf{x}, t) = -j\gamma f(t) \mathbf{g} \cdot \mathbf{x} M(\mathbf{x}, t) + \nabla \cdot (\mathcal{D}_0 \nabla M(\mathbf{x}, t)), \quad \mathbf{x} \in \Omega,$$

where  $\gamma = 267.513 \text{ rad } \mu\text{s}^{-1} T^{-1}$  is the gyromagnetic ratio of the water proton,  $j$  is the imaginary unit,  $\mathcal{D}_0$  is the intrinsic diffusion coefficient in the neuron compartment  $\Omega$ . The magnetization is a function of position  $\mathbf{x}$  and time  $t$ , and depends on the diffusion gradient vector  $\mathbf{g}$  and the time profile  $f(t)$ .

A commonly used time profile (diffusion-encoding sequence) is the pulsed-gradient spin echo (PGSE) [32] sequence, with two rectangular pulses of duration  $\delta$ , separated by a time interval  $\Delta - \delta$ , for which the profile  $f(t)$  is

$$(3.2) \quad f(t) = \begin{cases} 1, & 0 \leq t \leq \delta, \\ -1, & \Delta < t \leq \Delta + \delta, \\ 0, & \text{otherwise.} \end{cases}$$

In the case that the rectangular pulses are narrow, i.e.,  $\delta \ll \Delta$ , this allows the Bloch-Torrey PDE to be transformed to the diffusion equation. This assumption is called the narrow pulse approximation [32] and it is taken up in [subsection 3.2](#).

The PDE in (3.1) needs boundary conditions. We assume negligible membrane permeability, meaning the zero Neumann boundary condition:

$$\mathcal{D}_0 \nabla M(\mathbf{x}, t) \cdot \mathbf{n} = 0, \quad \mathbf{x} \in \partial\Omega,$$

where  $\mathbf{n}$  is the unit outward pointing normal vector at  $\mathbf{x}$ . In addition, the PDE has the constant initial condition:

$$M(\mathbf{x}, 0) = \rho, \quad \mathbf{x} \in \Omega,$$

where  $\rho$  is the initial spin density.

The diffusion MRI signal is measured at echo time  $t = T_E \geq \Delta + \delta$  for PGSE. This signal is the integral of  $M(\mathbf{x}, T_E)$ :

$$s \equiv \int_{\mathbf{x} \in \bigcup \{\Omega\}} M(\mathbf{x}, T_E) d\mathbf{x},$$

where  $\bigcup \{\Omega\}$  represents a set of biological compartments with impermeable membranes.

The signal  $s$  is usually plotted against a quantity called the b-value [32, 27]. The b-value depends on  $\mathbf{g}$  and  $f(t)$  and is defined as

$$b(\mathbf{g}) = \gamma^2 \|\mathbf{g}\|^2 \int_0^{T_E} du \left( \int_0^u f(s) ds \right)^2.$$

For PGSE, the b-value is [32]:

$$(3.3) \quad b(\mathbf{g}, \delta, \Delta) = \gamma^2 \|\mathbf{g}\|^2 \delta^2 (\Delta - \delta/3).$$

The reason for these definitions is that in a homogeneous medium, the signal attenuation is  $e^{-\mathcal{D}_0 b}$ , where  $\mathcal{D}_0$  is the intrinsic diffusion coefficient.

**3.2. Narrow pulse approximation.** In this paper, we restrict ourselves to simplified conditions on the diffusion-encoding gradient, specifically, we derive our method under the narrow pulse assumption, where the pulse duration is very short compared to the delay between the pulses [32], i.e.,  $\delta \ll \Delta$ . This will lead to the solution of a diffusion equation instead of the more complicated Bloch-Torrey PDE, as explained below.

Let us consider spins initially located at  $\mathbf{x}$ . After the first pulse, the complex phase of these spins is  $e^{-j\delta\gamma\mathbf{g}\cdot\mathbf{x}}$ . This means the complex magnetization at  $t = \delta$  due to a uniform distribution of initial spins with density  $\rho$  can be written as:

$$M(\mathbf{x}, \delta) \approx \rho e^{-j\delta\gamma\mathbf{g}\cdot\mathbf{x}}, \quad \mathbf{x} \in \Omega.$$

Because the gradient magnetic field is turned off after the first pulse, the spins move but the phase of the spins does not change. Therefore, the magnetization between pulses satisfies the diffusion equation:

$$(3.4) \quad \frac{\partial}{\partial t} M(\mathbf{x}, t) = \nabla \cdot (\mathcal{D}_0 \nabla M(\mathbf{x}, t)), \quad \mathbf{x} \in \Omega, t \in [\delta, \Delta],$$

subject to the zero Neumann boundary condition:

$$(3.5) \quad \mathcal{D}_0 \nabla M(\mathbf{x}_0, t) \cdot \mathbf{n} = 0, \quad \mathbf{x}_0 \in \partial\Omega, t \in [\delta, \Delta],$$

where  $\mathbf{n}$  is the unit outward pointing normal vector at  $\mathbf{x}_0$ , and initial condition at  $t = \delta$  is:

$$(3.6) \quad M(\mathbf{x}, \delta) = \rho e^{-j\delta\gamma\mathbf{g}\cdot\mathbf{x}}, \quad \mathbf{x} \in \Omega.$$

During the second pulse, at the point  $\mathbf{x}$ , the additional accumulated complex phase is  $e^{j\delta\gamma\mathbf{g}\cdot\mathbf{x}}$ , so the magnetization at the position  $\mathbf{x}$  and time  $TE$  is:

$$(3.7) \quad M(\mathbf{x}, TE) \approx M(\mathbf{x}, \Delta) e^{j\delta\gamma\mathbf{g}\cdot\mathbf{x}}, \quad \mathbf{x} \in \Omega.$$

We emphasize again that we used the assumption  $\delta \ll \Delta$ . The echo-time  $TE$  is usually some time after the end of the second pulse (i.e.  $TE \geq \Delta + \delta$ ).

The diffusion MRI signal  $s$  is the total magnetization measured at the echo time:

$$(3.8) \quad s = \int_{\mathbf{x} \in \Omega} M(\mathbf{x}, \Delta) e^{j\delta\gamma\mathbf{g}\cdot\mathbf{x}} d\mathbf{x}.$$

**4. Methodology.** We derive our new method below.

#### 4.1. Solution of the diffusion equation and the diffusion MRI signal.

Before we solve the diffusion equation using potential theory, we transform the initial and boundary conditions. We transform the diffusion equation in (3.4)–(3.6) such that it is subject to zero initial conditions and complex-valued non-zero Neumann boundary conditions. Define

$$(4.1) \quad \omega(\mathbf{x}, t) \equiv M(\mathbf{x}, t + \delta) - \rho e^{-4\pi^2 \mathcal{D}_0 \|\mathbf{q}\|^2 t} e^{-2\pi j \mathbf{q} \cdot \mathbf{x}}, \quad \mathbf{x} \in \Omega, t \in [0, \Delta - \delta],$$

where  $\mathbf{q} = \delta \gamma \mathbf{g} / 2\pi$ . We will work on the quantity  $\omega(\mathbf{x}, t)$  in (4.1), which satisfies the diffusion equation:

$$(4.2) \quad \frac{\partial}{\partial t} \omega(\mathbf{x}, t) = \nabla \cdot (\mathcal{D}_0 \nabla \omega(\mathbf{x}, t)), \quad \mathbf{x} \in \Omega, t \in [0, \Delta - \delta],$$

subject to non-homogeneous Neumann boundary conditions:

$$(4.3) \quad \mathcal{D}_0 \nabla \omega(\mathbf{x}_0, t) \cdot \mathbf{n} = \mathcal{D}_0 \mathcal{N}(\mathbf{x}_0, t, \mathbf{q}) \quad \mathbf{x}_0 \in \partial\Omega, t \in [0, \Delta - \delta],$$

and zero initial conditions:

$$(4.4) \quad \omega(\mathbf{x}, 0) = 0, \quad \mathbf{x} \in \Omega.$$

The Neumann forcing term is complex-valued, periodic in space in the direction  $\mathbf{q}$ , and decays exponentially in time:

$$(4.5) \quad \mathcal{N}(\mathbf{x}, t, \mathbf{q}) \equiv 2\pi \rho \mathbf{q} \cdot \mathbf{n} (j e^{-2\pi j \mathbf{q} \cdot \mathbf{x}}) e^{-4\pi^2 \mathcal{D}_0 \|\mathbf{q}\|^2 t}.$$

The diffusion MRI signal  $s$  can be reformulated in terms of  $\omega$ :

$$(4.6) \quad s = |\Omega| \rho e^{-4\pi^2 \mathcal{D}_0 \|\mathbf{q}\|^2 (\Delta - \delta)} + \int_{\mathbf{x} \in \Omega} \omega(\mathbf{x}, \Delta - \delta) e^{2\pi j \mathbf{q} \cdot \mathbf{x}} d\mathbf{x}.$$

In the above, the first term is explicit, the second term needs to be computed. We define a time dependent integral whose value at  $t = \Delta - \delta$  gives second term:

$$(4.7) \quad \bar{\omega}(\mathbf{q}, t) \equiv \int_{\mathbf{x} \in \Omega} \omega(\mathbf{x}, t) e^{2\pi j \mathbf{q} \cdot \mathbf{x}} d\mathbf{x}, \quad t \in [0, \Delta - \delta].$$

The function  $\bar{\omega}$  can be expanded by the Green's second identity:

$$\begin{aligned} \bar{\omega}(\mathbf{q}, t) &= \frac{-1}{4\pi^2 \mathcal{D}_0 \|\mathbf{q}\|^2} \left( \int_{\Omega} \nabla \cdot (\mathcal{D}_0 \nabla \omega(\mathbf{x}, t)) e^{2\pi j \mathbf{q} \cdot \mathbf{x}} d\mathbf{x} + B \right), \\ B &= \int_{\partial\Omega} 2\pi j \mathcal{D}_0 \mathbf{q} \cdot \mathbf{n} \omega(\mathbf{x}, t) e^{2\pi j \mathbf{q} \cdot \mathbf{x}} ds_{\mathbf{x}} - \int_{\partial\Omega} \mathcal{D}_0 \nabla \omega(\mathbf{x}, t) \cdot \mathbf{n} e^{2\pi j \mathbf{q} \cdot \mathbf{x}} ds_{\mathbf{x}}. \end{aligned}$$

Using the diffusion equation and the nonhomogeneous Neumann boundary conditions, we get an ordinary differential equation for  $\bar{\omega}$ :

$$(4.8) \quad \frac{d}{dt} \bar{\omega}(\mathbf{q}, t) = -4\pi^2 \mathcal{D}_0 \|\mathbf{q}\|^2 \bar{\omega}(\mathbf{q}, t) - 2\pi j \mathcal{D}_0 \int_{\partial\Omega} \mathbf{q} \cdot \mathbf{n} \omega(\mathbf{x}, t) e^{2\pi j \mathbf{q} \cdot \mathbf{x}} ds_{\mathbf{x}},$$

which has an analytical solution:

$$\begin{aligned} \bar{\omega}(\mathbf{q}, t) &= -\mathcal{D}_0 \int_{\partial\Omega} \int_0^t 2\pi j \mathbf{q} \cdot \mathbf{n} e^{-4\pi^2 \mathcal{D}_0 \|\mathbf{q}\|^2 (t-\tau)} \omega(\mathbf{x}, \tau) e^{2\pi j \mathbf{q} \cdot \mathbf{x}} d\tau ds_{\mathbf{x}}, \\ (4.9) \quad &= \mathcal{D}_0 \rho^{-1} \int_{\partial\Omega} \int_0^t \mathcal{N}^*(\mathbf{x}, t - \tau, \mathbf{q}) \omega(\mathbf{x}, \tau) d\tau ds_{\mathbf{x}}. \end{aligned}$$

The asterisk symbol  $*$  denotes the complex conjugation. It can be proved that (4.9) satisfies a recursive relationship in time:

(4.10)

$$\bar{\omega}(\mathbf{q}, t) = e^{-4\pi^2 \mathcal{D}_0 \|\mathbf{q}\|^2 \Delta t} \bar{\omega}(\mathbf{q}, t - \Delta t) + \mathcal{D}_0 \rho^{-1} \int_{\partial\Omega} \int_{t-\Delta t}^t \mathcal{N}^*(\mathbf{x}, t - \tau, \mathbf{q}) \omega(\mathbf{x}, \tau) d\tau ds_{\mathbf{x}}.$$

Equation (4.7) and (4.9) are mathematically equivalent for evaluating the diffusion MRI signal (at  $t = \Delta - \delta$ ). It can be seen that, while (4.7) requires the value of  $\omega$  on the entire domain  $\Omega$ , (4.9) only needs the value of  $\omega$  on the boundary, which is more computationally efficient. The recursion in time above also increases the computational efficiency. We will use the method of layer potentials to get the boundary values in the next section.

**4.2. The single layer potential representation.** The PDE in (4.2)–(4.4) has Neumann boundary conditions, zero initial conditions and zero forcing term, allowing us to represent the solution  $\omega(\mathbf{x}, t)$  as a single layer potential, with a density function  $\mu$  defined on  $\partial\Omega$  [9]. In other words,  $\omega(\mathbf{x}, t) = S[\mu](\mathbf{x}, t)$ . The definition for the single layer potential is

$$(4.11) \quad \omega(\mathbf{x}, t) = S[\mu](\mathbf{x}, t) \equiv \int_0^t \int_{\partial\Omega} \mathcal{D}_0 G(\mathbf{x} - \mathbf{y}, t - \tau) \mu(\mathbf{y}, \tau) ds_{\mathbf{y}} d\tau,$$

where  $G(\mathbf{x}, t)$  is the fundamental solution of the 2D diffusion equation in a box  $[-L_1/2, L_1/2] \times [-L_2/2, L_2/2]$ , with periodic boundary conditions. The fundamental solution  $G(\mathbf{x}, t)$  has two equivalent representations [8]:

$$(4.12) \quad G_{Gauss}(\mathbf{x}, t) = (4\pi \mathcal{D}_0 t)^{-1} \sum_{\mathbf{z} \in \mathbb{Z}^2} e^{-\frac{\|\mathbf{x} - \mathbf{z} \odot \mathbf{L}\|^2}{4\mathcal{D}_0 t}},$$

$$(4.13) \quad G_{Fourier}(\mathbf{x}, t) = \frac{1}{L_1 L_2} \sum_{\substack{\boldsymbol{\nu} = \mathbf{z} \oslash \mathbf{L} \\ \mathbf{z} \in \mathbb{Z}^2}} e^{-4\pi^2 \mathcal{D}_0 \|\boldsymbol{\nu}\|^2 t} e^{2\pi j \boldsymbol{\nu} \cdot \mathbf{x}},$$

where  $\odot$  and  $\oslash$  are hadamard product and hadamard division, respectively, and  $\mathbf{L} = [L_1, L_2]^T$ . For the convenience of notation, in the following, we set  $L_1 = L_2 = L$  and note by  $\Delta\nu = \frac{1}{L}$ . In this way, we rewrite (4.13) as

$$(4.14) \quad G_{Fourier}(\mathbf{x}, t) = \sum_{\substack{\boldsymbol{\nu} = \mathbf{z} \oslash \mathbf{L} \\ \mathbf{z} \in \mathbb{Z}^2}} e^{-4\pi^2 \mathcal{D}_0 \|\boldsymbol{\nu}\|^2 t} e^{2\pi j \boldsymbol{\nu} \cdot \mathbf{x}} \Delta\nu^2$$

in order to recall its relationship with the Fourier transform. The imposition of periodic boundary conditions on the faces of the box allows us to use the discrete Fourier series.

The density function  $\mu$  is chosen to be a causal function and is determined by imposing the Neumann boundary conditions on the geometry boundary  $\partial\Omega$  [16]:

$$\lim_{\mathbf{x} \rightarrow \mathbf{x}_0 \in \partial\Omega} \nabla S[\mu](\mathbf{x}, t) \cdot \mathbf{n} = \mathcal{N}(\mathbf{x}_0, t, \mathbf{q}), \quad \mathbf{x}_0 \in \partial\Omega, t \in [0, \Delta - \delta].$$

Using the jump property of the trace of the double layer potential, the integral equation to be solved for  $\mu$  is then the following:

$$(4.15) \quad \frac{1}{2}\mu(\mathbf{x}_0, t) + K[\mu](\mathbf{x}_0, t) = \mathcal{N}(\mathbf{x}_0, t, \mathbf{q}), \quad \mathbf{x}_0 \in \partial\Omega, t \in [0, \Delta - \delta],$$

with

$$(4.16) \quad K[\mu](\mathbf{x}_0, t) \equiv \int_0^t \int_{\partial\Omega} \mathcal{D}_0 \frac{\partial G}{\partial \mathbf{n}_{\mathbf{x}_0}}(\mathbf{x}_0 - \mathbf{y}, t - \tau) \mu(\mathbf{y}, \tau) ds_{\mathbf{y}} d\tau$$

being the principal value integral on the boundary. Solving the integral equation (4.15) for  $\mu$  plays the pivotal role in our method. We present the detailed steps in the next sections.

### 4.3. Splitting the single layer potential into local and history parts.

The single layer potential  $S[\mu]$  is split into a history part,  $S_{long}[\mu]$ , and a local in time part,  $S_{short}[\mu]$ . Since the local in time part  $S_{short}[\mu]$  contains the singularity of the fundamental solution  $G$ , we approximate it by asymptotic formulas. The asymptotic trace formulas are only accurate in an interval near the singularity, so we limit their use to the interval  $[t - \eta, t]$ , with  $\eta$  being a small quantity to be determined later. In other words,

$$(4.17) \quad S[\mu](\mathbf{x}, t) = S_{short}[\mu](\mathbf{x}, t) + S_{long}[\mu](\mathbf{x}, t),$$

with

$$(4.18) \quad \begin{aligned} S_{short}[\mu](\mathbf{x}, t) &:= \int_{t-\eta}^t \int_{\partial\Omega} \mathcal{D}_0 G_{Gauss}(\mathbf{x} - \mathbf{y}, t - \tau) \mu(\mathbf{y}, \tau) ds_{\mathbf{y}} d\tau, \\ S_{long}[\mu](\mathbf{x}, t) &:= \int_0^{t-\eta} \int_{\partial\Omega} \mathcal{D}_0 G_{Fourier}(\mathbf{x} - \mathbf{y}, t - \tau) \mu(\mathbf{y}, \tau) ds_{\mathbf{y}} d\tau. \end{aligned}$$

Similarly, we decompose  $K[\mu]$  into 2 parts:

$$(4.19) \quad K[\mu](\mathbf{x}_0, t) = K_{short}[\mu](\mathbf{x}_0, t) + K_{long}[\mu](\mathbf{x}_0, t),$$

with

$$(4.20) \quad \begin{aligned} K_{short}[\mu](\mathbf{x}_0, t) &:= \int_{t-\eta}^t \int_{\partial\Omega} \mathcal{D}_0 \frac{\partial G_{Gauss}}{\partial \mathbf{n}_{\mathbf{x}_0}}(\mathbf{x}_0 - \mathbf{y}, t - \tau) \mu(\mathbf{y}, \tau) ds_{\mathbf{y}} d\tau, \\ K_{long}[\mu](\mathbf{x}_0, t) &:= \int_0^{t-\eta} \int_{\partial\Omega} \mathcal{D}_0 \frac{\partial G_{Fourier}}{\partial \mathbf{n}_{\mathbf{x}_0}}(\mathbf{x}_0 - \mathbf{y}, t - \tau) \mu(\mathbf{y}, \tau) ds_{\mathbf{y}} d\tau. \end{aligned}$$

Next, we compute or approximate the above history and local parts.

**4.3.1. Asymptotic trace formulas for the local part.** Based on the expressions derived in [8], the asymptotic trace formulas in two dimensions for the local parts, when  $t > \eta$ , are:

$$(4.21) \quad S_{short}[\mu](\mathbf{x}_0, t) = \sqrt{\frac{\mathcal{D}_0 \eta}{\pi}} \mu(\mathbf{x}_0, t) + O(\eta^{3/2}), t > \eta$$

and

$$(4.22) \quad K_{short}[\mu](\mathbf{x}_0, t) = -\frac{\sqrt{\mathcal{D}_0 \eta}}{2\sqrt{\pi}} \kappa(\mathbf{x}_0) \mu(\mathbf{x}_0, t) + O(\eta^{3/2}), t > \eta,$$



where  $\kappa(\mathbf{x}_0)$  is the curvature at the point  $\mathbf{x}_0 \in \partial\Omega$ . The boundary  $\partial\Omega$ , which models the cell membrane, is a closed 2D plane curve. We assume it is twice differentiable. Let  $\psi(\alpha) = (x(\alpha), y(\alpha))$  be a parametric representation of  $\partial\Omega$ . We choose a general parameter  $\alpha$  such that  $\psi(\alpha)$  is oriented counterclockwise. The curvature at the point  $\mathbf{x}_0 = \psi(\alpha_0)$  is defined as

$$(4.23) \quad \kappa(\mathbf{x}_0) = \frac{x'y'' - y'x''}{(x'^2 + y'^2)^{3/2}} \Big|_{\alpha=\alpha_0},$$

where primes refer to derivatives with respect to  $\alpha$ .

We also need to initialize values for  $t \leq \eta$ . It has been derived in [9] that the expressions are:

$$(4.24) \quad S_{short}[\mu](\mathbf{x}_0, t) = \sqrt{\frac{\mathcal{D}_0 t}{\pi}} \mu(\mathbf{x}_0, t) + O(t^{3/2}), t \leq \eta,$$

and

$$(4.25) \quad K_{short}[\mu](\mathbf{x}_0, t) = -\frac{\sqrt{\mathcal{D}_0 t}}{2\sqrt{\pi}} \kappa(\mathbf{x}_0) \mu(\mathbf{x}_0, t) + O(t^{3/2}), t \leq \eta.$$

**4.3.2. Fourier representation of history part.** For the smooth part of the single layer potential, a Fourier representation for the Dirichlet trace is proposed in [8]:

$$(4.26) \quad S_{long}[\mu](\mathbf{x}_0, t) = \mathcal{D}_0 \sum_{\substack{\boldsymbol{\nu}=\mathbf{z} \odot \mathbf{L} \\ \mathbf{z} \in \mathbb{Z}^2}} \hat{f}(\boldsymbol{\nu}, t) e^{2\pi j \boldsymbol{\nu} \cdot \mathbf{x}_0} \Delta \nu^2,$$

and the Neumann trace is

$$(4.27) \quad K_{long}[\mu](\mathbf{x}_0, t) = \mathcal{D}_0 \sum_{\substack{\boldsymbol{\nu}=\mathbf{z} \odot \mathbf{L} \\ \mathbf{z} \in \mathbb{Z}^2}} 2\pi j \boldsymbol{\nu} \cdot \mathbf{n} \hat{f}(\boldsymbol{\nu}, t) e^{2\pi j \boldsymbol{\nu} \cdot \mathbf{x}_0} \Delta \nu^2,$$

where the Fourier coefficients are

$$(4.28) \quad \hat{f}(\boldsymbol{\nu}, t) = \int_0^{t-\eta} \int_{\partial\Omega} e^{-4\pi^2 \mathcal{D}_0 \|\boldsymbol{\nu}\|^2 (t-\tau)} \mu(\mathbf{y}, \tau) e^{-2\pi j \boldsymbol{\nu} \cdot \mathbf{y}} d\mathbf{s}_{\mathbf{y}} d\tau.$$

To avoid history dependent time integration, we use the following recurrence formula for the Fourier coefficients

$$(4.29) \quad \hat{f}(\boldsymbol{\nu}, t) = e^{-4\pi^2 \mathcal{D}_0 \|\boldsymbol{\nu}\|^2 \Delta t} \hat{f}(\boldsymbol{\nu}, t - \Delta t) + \int_{t-\eta-\Delta t}^{t-\eta} \int_{\partial\Omega} e^{-4\pi^2 \mathcal{D}_0 \|\boldsymbol{\nu}\|^2 (t-\tau)} \mu(\mathbf{y}, \tau) e^{-2\pi j \boldsymbol{\nu} \cdot \mathbf{y}} d\mathbf{s}_{\mathbf{y}} d\tau,$$

so only local-in-time integrals are needed at each time step.

The above formulas hold when  $t > \eta$ . For  $t \leq \eta$ , we initialize  $S_{long}[\mu]$ ,  $K_{long}[\mu]$ , and  $\hat{f}$  to be 0.

**4.4. Computation of the single layer density.** Based on the decomposition of the single layer potential and the approximation of the history and the local parts detailed previously, we can compute the density function  $\mu$ .

For  $t \leq \eta$ , substituting (4.25) into (4.15) and solving the integral equation, we can get the approximation to the density

$$(4.30) \quad \mu(\mathbf{x}_0, t) = \frac{2\mathcal{N}(\mathbf{x}_0, t, \mathbf{q})}{1 - \sqrt{\frac{\mathcal{D}_0 t}{\pi}} \kappa(\mathbf{x}_0)} + O(t^{3/2}), \quad \mathbf{x}_0 \in \partial\Omega, \quad t \leq \eta.$$

For  $t \in (\eta, \Delta - \delta]$ , the integral equation (4.15) can be rewritten as

$$\frac{1}{2}\mu(\mathbf{x}_0, t) + K_{short}[\mu](\mathbf{x}_0, t) = \beta(\mathbf{x}_0, t),$$

where the right hand side is

$$(4.31) \quad \beta(\mathbf{x}_0, t) \equiv -K_{long}[\mu](\mathbf{x}_0, t) + \mathcal{N}(\mathbf{x}_0, t, \mathbf{q}).$$

We write the solution of the above integral equation as

$$(4.32) \quad \mu(\mathbf{x}_0, t) = 2(I + 2K_{short})^{-1}[\beta](\mathbf{x}_0, t), \quad \mathbf{x}_0 \in \partial\Omega, t \in (\eta, \Delta - \delta],$$

and expand the operator  $(I + 2K_{short})^{-1}$  (corresponding to  $K_{short}$  being a contraction) as

$$(4.33) \quad \mu(\mathbf{x}_0, t) = 2(I - 2K_{short} + 4K_{short}^2 - \dots + (-2)^n K_{short}^n + \dots)[\beta](\mathbf{x}_0, t).$$

We approximate  $K_{short}^n[\beta]$  using (4.22) and we get

$$(4.34) \quad K_{short}^n[\beta](\mathbf{x}_0, t) = \frac{1}{(-2)^n} \left( \frac{\mathcal{D}_0 \eta}{\pi} \right)^{n/2} \kappa^n(\mathbf{x}_0) \beta(\mathbf{x}_0, t) + O(\eta^{3/2}).$$

Then, we keep all terms of the operator expansion to obtain

$$(4.35) \quad \begin{aligned} \mu(\mathbf{x}_0, t) &= 2(\beta(\mathbf{x}_0, t) - 2K_{short}[\beta](\mathbf{x}_0, t) + 4K_{short}^2[\beta](\mathbf{x}_0, t) - \dots) \\ &= 2\beta(\mathbf{x}_0, t) \left( 1 + \left( \frac{\mathcal{D}_0 \eta}{\pi} \right)^{\frac{1}{2}} \kappa(\mathbf{x}_0) + \frac{\mathcal{D}_0 \eta}{\pi} \kappa^2(\mathbf{x}_0) + \dots \right) + O(\eta^{3/2}) \\ &= 2\beta(\mathbf{x}_0, t) / \left( 1 - \sqrt{\frac{\mathcal{D}_0 \eta}{\pi}} \kappa(\mathbf{x}_0) \right) + O(\eta^{3/2}). \end{aligned}$$

**4.5. Computation of the single layer potential.** Once the density  $\mu$  is obtained, we compute the single layer potential  $S[\mu]$  in the following way.

When  $t \leq \eta$ , the expression for the single layer potential is

$$\begin{aligned} S[\mu](\mathbf{x}_0, t) &= S_{short}[\mu](\mathbf{x}_0, t) \\ &= \sqrt{\frac{\mathcal{D}_0 t}{\pi}} \frac{4\pi j \rho \mathbf{q} \cdot \mathbf{n} e^{-4\pi^2 \mathcal{D}_0 \|\mathbf{q}\|^2 t} e^{-2\pi j \mathbf{q} \cdot \mathbf{x}_0}}{1 - \sqrt{\frac{\mathcal{D}_0 t}{\pi}} \kappa(\mathbf{x}_0)} + O(t^{3/2}), \quad \mathbf{x}_0 \in \partial\Omega, t \in [0, \eta]. \end{aligned}$$

For  $t \in (\eta, \Delta - \delta]$ , the single layer potential has both a local part and a history part. The local part is

$$S_{short}[\mu](\mathbf{x}_0, t) = \sqrt{\frac{\mathcal{D}_0 \eta}{\pi}} \mu(\mathbf{x}_0, t) + O(\eta^{3/2}), \quad \mathbf{x}_0 \in \partial\Omega, t \in (\eta, \Delta - \delta].$$

As for the history part  $S_{long}[\mu]$ , it can be approximated by the truncated Fourier series:

(4.36)

$$S_{long}[\mu](\mathbf{x}_0, t) = \mathcal{D}_0 \sum_{\boldsymbol{\nu}=-\boldsymbol{\nu}_{max}}^{\boldsymbol{\nu}_{max}} \hat{f}(\boldsymbol{\nu}, t) e^{2\pi j \boldsymbol{\nu} \cdot \mathbf{x}_0} \Delta \nu^2 + E(\nu_{max}), \quad \mathbf{x}_0 \in \partial\Omega, t \in (\eta, \Delta - \delta].$$

In the above, we denote the error term due to truncating the infinite Fourier series up to  $\nu_{max}$  by  $E(\nu_{max})$ . We do not have an analytical expression for  $E(\nu_{max})$ , but we will show later in the numerical results that it decays exponentially in  $\nu_{max}$ .

The addition of  $S_{short}[\mu]$  and  $S_{long}[\mu]$  gives the single layer potential  $S[\mu]$  which is the solution of (4.2) on the boundary:

$$S[\mu](\mathbf{x}_0, t) = S_{short}[\mu](\mathbf{x}_0, t) + S_{long}[\mu](\mathbf{x}_0, t), \quad \mathbf{x}_0 \in \partial\Omega, t \in [0, \Delta - \delta].$$

At the current iteration step, the Fourier coefficients  $\hat{f}$  that are still unknown, will be computed using the density function  $\mu$  from the previous iterations, as explained in the following.

**4.5.1. Computation of the Fourier coefficients of the history part.** For  $t \leq \eta$ ,  $\hat{f}$  is set to zero, as well as  $K_{long}[\mu]$ . For  $t \in (\eta, 2\eta]$ ,  $\hat{f}$  are computed using the density  $\mu$  from the previous iterations:

(4.37)

$$\begin{aligned} \hat{f}(\boldsymbol{\nu}, t) = & e^{-4\pi^2 \mathcal{D}_0 \|\boldsymbol{\nu}\|^2 \Delta t} \hat{f}(\boldsymbol{\nu}, t - \Delta t) + \\ & \underbrace{\int_{\partial\Omega} \int_{t-\eta-\Delta t}^{t-\eta} e^{-4\pi^2 \mathcal{D}_0 \|\boldsymbol{\nu}\|^2 (t-\tau)} e^{-2\pi j \boldsymbol{\nu} \cdot \mathbf{y}} \mu(\mathbf{y}, \tau) d\tau ds_{\mathbf{y}},}_{\hat{f}_{temp1}(\boldsymbol{\nu}, t)} \quad \boldsymbol{\nu} \in [-\nu_{max}, \nu_{max}]^2, \end{aligned}$$

with

$$\hat{f}_{temp1}(\boldsymbol{\nu}, t) = \int_{\partial\Omega} 4\pi j \mathbf{q} \cdot \mathbf{n} e^{-2\pi j (\mathbf{q} + \boldsymbol{\nu}) \cdot \mathbf{y}} \underbrace{\int_{t-\eta-\Delta t}^{t-\eta} \frac{e^{-4\pi^2 \mathcal{D}_0 [\|\boldsymbol{\nu}\|^2 (t-\tau) + \|\mathbf{q}\|^2 \tau]}}{1 - \sqrt{\frac{\mathcal{D}_0 \tau}{\pi}} \kappa(\mathbf{y})} d\tau ds_{\mathbf{y}}}_{p}.$$

We apply the trapezoidal rule to the time integration  $p$  to obtain

$$p = \begin{cases} -\frac{2\pi e^{-4\pi^2 \mathcal{D}_0 \|\mathbf{q}\|^2 t}}{\mathcal{D}_0 \kappa^2(\mathbf{y})} \left[ \kappa(\mathbf{y}) \sqrt{\frac{\mathcal{D}_0}{\pi}} (\sqrt{t-\eta} - \sqrt{t-\eta-\Delta t}) + \ln \left( \frac{1 - \kappa(\mathbf{y}) \sqrt{\frac{\mathcal{D}_0}{\pi} (t-\eta)}}{1 - \kappa(\mathbf{y}) \sqrt{\frac{\mathcal{D}_0}{\pi} (t-\eta-\Delta t)}} \right) \right], & \|\boldsymbol{\nu}\| = \|\mathbf{q}\|; \\ e^{-4\pi^2 \mathcal{D}_0 [\|\mathbf{q}\|^2 (t-\eta) + \|\boldsymbol{\nu}\|^2 \eta]} \left[ \frac{1 + e^{4\pi^2 \mathcal{D}_0 (\|\mathbf{q}\|^2 - \|\boldsymbol{\nu}\|^2) \Delta t} (4\pi^2 \mathcal{D}_0 (\|\mathbf{q}\|^2 - \|\boldsymbol{\nu}\|^2) \Delta t - 1)}{\Delta t (4\pi^2 \mathcal{D}_0 (\|\mathbf{q}\|^2 - \|\boldsymbol{\nu}\|^2))^2 \left( 1 - \kappa(\mathbf{y}) \sqrt{\frac{\mathcal{D}_0}{\pi} (t-\eta-\Delta t)} \right)} + \frac{e^{4\pi^2 \mathcal{D}_0 (\|\mathbf{q}\|^2 - \|\boldsymbol{\nu}\|^2) \Delta t} - 4\pi^2 \mathcal{D}_0 (\|\mathbf{q}\|^2 - \|\boldsymbol{\nu}\|^2) \Delta t - 1}{\Delta t (4\pi^2 \mathcal{D}_0 (\|\mathbf{q}\|^2 - \|\boldsymbol{\nu}\|^2))^2 \left( 1 - \kappa(\mathbf{y}) \sqrt{\frac{\mathcal{D}_0}{\pi} (t-\eta)} \right)} \right], & \|\boldsymbol{\nu}\| \neq \|\mathbf{q}\|. \end{cases}$$

Once we compute the time integration  $p$ , the integration over the boundary  $\partial\Omega$  can be approximated by uniform discretization in arc length.

Remaining on  $t \in (\eta, 2\eta]$ , next we compute the long time part  $K_{long}[\mu]$  via the Fourier series

$$K_{long}[\mu](\mathbf{x}_0, t) = \mathcal{D}_0 \sum_{\boldsymbol{\nu}=-\boldsymbol{\nu}_{max}}^{\boldsymbol{\nu}_{max}} 2\pi j \boldsymbol{\nu} \cdot \mathbf{n} \hat{f}(\boldsymbol{\nu}, t) e^{2\pi j \boldsymbol{\nu} \cdot \mathbf{x}_0} \Delta \nu^2 + E(\nu_{max}).$$

With a slight abuse of notation, we use the same notation  $E(\nu_{max})$  as in (4.36) for the error due to truncating the Fourier series at  $\nu_{max}$ .

Finally, the density function  $\mu$  for (the current time)  $t \in (\eta, 2\eta]$  is computed as:

$$\mu(\mathbf{x}_0, t) = \frac{2[\mathcal{N}(\mathbf{x}_0, t) - K_{long}[\mu](\mathbf{x}_0, t)]}{1 - \sqrt{\frac{\mathcal{D}_0 \eta}{\pi}} \kappa(\mathbf{x}_0)} + O(\eta^{3/2}).$$

On the rest of the time interval,  $t \in (2\eta, \Delta - \delta]$ ,  $\hat{f}$  still uses the density  $\mu$  from previous iterations, but the formulas are different:

(4.38)

$$\hat{f}(\boldsymbol{\nu}, t) = e^{-4\pi^2 \mathcal{D}_0 \|\boldsymbol{\nu}\|^2 \Delta t} \hat{f}(\boldsymbol{\nu}, t - \Delta t) + \underbrace{\int_{\partial\Omega} \int_{t-\eta-\Delta t}^{t-\eta} e^{-4\pi^2 \mathcal{D}_0 \|\boldsymbol{\nu}\|^2 (t-\tau)} e^{-2\pi j \boldsymbol{\nu} \cdot \mathbf{y}} \mu(\mathbf{y}, \tau) d\tau ds_{\mathbf{y}},}_{\hat{f}_{temp2}(\boldsymbol{\nu}, t)} \quad \boldsymbol{\nu} \in [-\nu_{max}, \nu_{max}]^2.$$

In the above, the Fourier coefficients  $\hat{f}(\boldsymbol{\nu}, t - \Delta t)$  at the previous time step are known, and the expression of  $\mu(\mathbf{x}_0, \tau)$  for  $\tau \in (\eta, \Delta - \delta - \eta]$  is

$$\mu(\mathbf{x}_0, \tau) = 2 \left( 1 - \sqrt{\frac{\mathcal{D}_0 \eta}{\pi}} \kappa(\mathbf{x}_0) \right)^{-1} [\mathcal{N}(\mathbf{x}_0, \tau) - K_{long}[\mu](\mathbf{x}_0, \tau)], \quad \mathbf{x}_0 \in \partial\Omega.$$

The integration on the right hand side of (4.38) is noted as  $\hat{f}_{temp2}(\boldsymbol{\nu}, t)$  in which we substitute the expression of  $\mu$  above. We split  $\hat{f}_{temp2}$  into two parts and gather the terms that are independent of time

$$\begin{aligned} \hat{f}_{temp2}(\boldsymbol{\nu}, t) &= \int_{\partial\Omega} 2 \left( 1 - \sqrt{\frac{\mathcal{D}_0 \eta}{\pi}} \kappa(\mathbf{y}) \right)^{-1} e^{-2\pi j \boldsymbol{\nu} \cdot \mathbf{y}} \times \\ &\quad (2\pi j \mathbf{q} \cdot \mathbf{n} e^{-2\pi j \mathbf{q} \cdot \mathbf{y}} \underbrace{\int_{t-\eta-\Delta t}^{t-\eta} e^{-4\pi^2 \mathcal{D}_0 (\|\mathbf{q}\|^2 \tau + \|\boldsymbol{\nu}\|^2 (t-\tau))} d\tau}_{h_1} - \\ &\quad \underbrace{\int_{t-\eta-\Delta t}^{t-\eta} K_{long}[\mu](\mathbf{y}, \tau) e^{-4\pi^2 \mathcal{D}_0 \|\boldsymbol{\nu}\|^2 (t-\tau)} d\tau}_{h_2}) ds_{\mathbf{y}}. \end{aligned}$$

The time integration  $h_1$  in the first part has an analytical expression

$$(4.39) \quad h_1 = \begin{cases} \Delta t \cdot e^{-4\pi^2 \mathcal{D}_0 \|\boldsymbol{\nu}\|^2 t} & \|\mathbf{q}\| = \|\boldsymbol{\nu}\| \\ e^{-4\pi^2 \mathcal{D}_0 [\|\mathbf{q}\|^2 (t-\eta) + \|\boldsymbol{\nu}\|^2 \eta]} \frac{e^{4\pi^2 \mathcal{D}_0 (\|\mathbf{q}\|^2 - \|\boldsymbol{\nu}\|^2) \Delta t} - 1}{4\pi^2 \mathcal{D}_0 (\|\mathbf{q}\|^2 - \|\boldsymbol{\nu}\|^2)} & \|\mathbf{q}\| \neq \|\boldsymbol{\nu}\| \end{cases}$$

The time integration  $h_2$  in the second part has to be calculated numerically. We apply the trapezoidal rule to  $K_{long}[\mu](\mathbf{y}, \tau)$  and we get

$$(4.40) \quad h_2 = \begin{cases} \frac{\Delta t}{2} [K_{long}[\mu](\mathbf{y}, t - \eta) + K_{long}[\mu](\mathbf{y}, t - \eta - \Delta t)] & \|\boldsymbol{\nu}\| = 0 \\ \left[ \frac{1 - e^{-4\pi^2 \mathcal{D}_0 \|\boldsymbol{\nu}\|^2 \Delta t} (4\pi^2 \mathcal{D}_0 \|\boldsymbol{\nu}\|^2 \Delta t + 1)}{(4\pi^2 \mathcal{D}_0 \|\boldsymbol{\nu}\|^2)^2 \Delta t} K_{long}[\mu](\mathbf{y}, t - \eta - \Delta t) + \right. \\ \left. \frac{e^{-4\pi^2 \mathcal{D}_0 \|\boldsymbol{\nu}\|^2 \Delta t} + 4\pi^2 \mathcal{D}_0 \|\boldsymbol{\nu}\|^2 \Delta t - 1}{(4\pi^2 \mathcal{D}_0 \|\boldsymbol{\nu}\|^2)^2 \Delta t} K_{long}[\mu](\mathbf{y}, t - \eta) \right] e^{-4\pi^2 \mathcal{D}_0 \|\boldsymbol{\nu}\|^2 \eta} & \|\boldsymbol{\nu}\| \neq 0 \end{cases}$$

The values of  $K_{long}[\mu]$  at time  $t - \eta - \Delta t$  and  $t - \eta$  have been computed in previous steps, thus the expressions for  $h_1$  and  $h_2$  can be computed in the current time step. Then we discretize uniformly in the arc length over the boundary to obtain  $\hat{f}_{temp2}$  as well as  $\hat{f}$ .

Staying on  $t \in (2\eta, \Delta - \delta]$ , it is straightforward to recover the long time part  $K_{long}[\mu]$  at time  $t$  by applying the inverse discrete Fourier transform

$$K_{long}[\mu](\mathbf{x}_0, t) = \mathcal{D}_0 \sum_{\boldsymbol{\nu}=-\boldsymbol{\nu}_{max}}^{\boldsymbol{\nu}_{max}} 2\pi j \boldsymbol{\nu} \cdot \mathbf{n} \hat{f}(\boldsymbol{\nu}, t) e^{2\pi j \boldsymbol{\nu} \cdot \mathbf{x}_0} \Delta \nu^2 + E(\nu_{max}).$$

Again, with a slight abuse of notation, we use the same notation  $E(\nu_{max})$  as in (4.36) for the error due to truncating the Fourier series at  $\nu_{max}$ . Finally, the density function  $\mu$  at the current time  $t$  is

$$\mu(\mathbf{x}_0, t) = \frac{2[\mathcal{N}(\mathbf{x}_0, t) - K_{long}[\mu](\mathbf{x}_0, t)]}{1 - \sqrt{\frac{\mathcal{D}_0 \eta}{\pi}} \kappa(\mathbf{x}_0)} + O(\eta^{3/2}),$$

which will be used for future iterations.

**4.6. Computation of the diffusion MRI signal.** After obtaining the single layer potential, the following procedure produces the diffusion MRI signal.

The diffusion MRI signal  $s$  has the representation

$$s = |\Omega| \rho e^{-4\pi^2 \mathcal{D}_0 \|\mathbf{q}\|^2 (\Delta - \delta)} + \bar{\omega}(\mathbf{q}, \Delta - \delta).$$

The quantity  $\bar{\omega}$  will be computed using the recursive relationship below (rewritten from (4.10)):

$$\begin{aligned} \bar{\omega}(\mathbf{q}, t) &= e^{-4\pi^2 \mathcal{D}_0 \|\mathbf{q}\|^2 \Delta t} \bar{\omega}(\mathbf{q}, t - \Delta t) \\ &\quad - \mathcal{D}_0 \int_{\partial\Omega} 2\pi j \mathbf{q} \cdot \mathbf{n} e^{2\pi j \mathbf{q} \cdot \mathbf{y}} \overbrace{\int_{t-\Delta t}^t e^{-4\pi^2 \mathcal{D}_0 \|\mathbf{q}\|^2 (t-\tau)} \omega(\mathbf{y}, \tau) d\tau}^u ds_{\mathbf{y}}. \end{aligned}$$

By applying the trapezoidal rule to the time integration  $u$ , we then get the expression

$$(4.41) \quad u = \begin{cases} \frac{\Delta t}{2} [\omega(\mathbf{y}, t - \Delta t) + \omega(\mathbf{y}, t)] & \|\mathbf{q}\| = 0 \\ \frac{1 - e^{-4\pi^2 \mathcal{D}_0 \|\mathbf{q}\|^2 \Delta t} (4\pi^2 \mathcal{D}_0 \|\mathbf{q}\|^2 \Delta t + 1)}{(4\pi^2 \mathcal{D}_0 \|\mathbf{q}\|^2)^2 \Delta t} \omega(\mathbf{y}, t - \Delta t) \\ + \frac{e^{-4\pi^2 \mathcal{D}_0 \|\mathbf{q}\|^2 \Delta t} + 4\pi^2 \mathcal{D}_0 \|\mathbf{q}\|^2 \Delta t - 1}{(4\pi^2 \mathcal{D}_0 \|\mathbf{q}\|^2)^2 \Delta t} \omega(\mathbf{y}, t) & \|\mathbf{q}\| \neq 0 \end{cases}$$

The variable  $\omega$  is the single layer potential  $S[\mu]$

$$\omega(\mathbf{x}_0, t) = S[\mu](\mathbf{x}_0, t) = S_{short}[\mu](\mathbf{x}_0, t) + S_{long}[\mu](\mathbf{x}_0, t).$$

The short time part has an asymptotic expression

$$S_{short}[\mu](\mathbf{x}_0, t) = 2\sqrt{\frac{\mathcal{D}_0\eta}{\pi}} \frac{\mathcal{N}(\mathbf{x}_0, t) - K_{long}[\mu](\mathbf{x}_0, t)}{1 - \sqrt{\frac{\mathcal{D}_0\eta}{\pi}}\kappa(\mathbf{x}_0)} + O(\eta^{3/2})$$

with

$$\mathcal{N}(\mathbf{x}_0, t) = 2\pi j\rho\mathbf{q} \cdot \mathbf{n} e^{-4\pi^2\mathcal{D}_0\|\mathbf{q}\|^2 t} e^{-2\pi j\mathbf{q} \cdot \mathbf{x}_0},$$

and

$$K_{long}[\mu](\mathbf{x}_0, t) = \mathcal{D}_0 \sum_{\nu=-\nu_{max}}^{\nu_{max}} 2\pi j\nu \cdot \mathbf{n} \hat{f}(\nu, t) e^{2\pi j\nu \cdot \mathbf{x}_0} \Delta\nu^2 + E(\nu_{max}).$$

The long time part is approximated by a Fourier series

$$S_{long}[\mu](\mathbf{x}_0, t) = \mathcal{D}_0 \sum_{\nu=-\nu_{max}}^{\nu_{max}} \hat{f}(\nu, t) e^{2\pi j\nu \cdot \mathbf{x}_0} \Delta\nu^2 + E(\nu_{max}).$$

Finally, a uniform arc length discretization of the boundary allows the numerical computation of  $\bar{\omega}$ .

#### REFERENCES

- [1] G. T. BALLS AND L. R. FRANK, A simulation environment for diffusion weighted mr experiments in complex media, Magn. Reson. Med., 62 (2009), pp. 771–778, <http://dx.doi.org/10.1002/mrm.22033>.
- [2] L. BELTRACHINI, Z. A. TAYLOR, AND A. F. FRANGI, A parametric finite element solution of the generalised bloch-torrey equation for arbitrary domains, Journal of Magnetic Resonance, 259 (2015), pp. 126 – 134, <https://doi.org/https://doi.org/10.1016/j.jmr.2015.08.008>, <http://www.sciencedirect.com/science/article/pii/S1090780715001743>.
- [3] L. M. BURCAW, E. FIEREMANS, AND D. S. NOVIKOV, Mesoscopic structure of neuronal tracts from time-dependent diffusion, NeuroImage, 114 (2015), pp. 18 – 37, <https://doi.org/10.1016/j.neuroimage.2015.03.061>.
- [4] P. COOK, Y. BAI, M. HALL, S. NEDJATI-GILANI, K. SEUNARINE, AND D. ALEXANDER, Camino: Diffusion mri reconstruction and processing, (2005).
- [5] C. FANG, V.-D. NGUYEN, D. WASSERMANN, AND J.-R. LI, Diffusion mri simulation of realistic neurons with spinductor and the neuron module, NeuroImage, 222 (2020), p. 117198.
- [6] D. GREBENKOV, Laplacian eigenfunctions in nmr. i. a numerical tool, Concepts in Magnetic Resonance Part A, 32A (2008), pp. 277–301, <https://doi.org/10.1002/cmr.a.20117>.
- [7] D. S. GREBENKOV, Laplacian eigenfunctions in nmr. ii. theoretical advances, Concepts Magn. Reson., 34A (2009), pp. 264–296, <https://doi.org/10.1002/cmr.a.20145>.
- [8] L. GREENGARD AND J. STRAIN, A fast algorithm for the evaluation of heat potentials, Comm. Pure Appl. Math., 43 (1990), pp. 949–963.
- [9] H. HADDAR, J.-R. LI, AND S. SCHIAVI, Understanding the time-dependent effective diffusion coefficient measured by diffusion mri: the intracellular case, SIAM Journal on Applied Mathematics, 78 (2018), pp. 774–800.
- [10] M. JALLAIS, P. L. RODRIGUES, A. GRAMFORT, AND D. WASSERMANN, Cytoarchitecture measurements in brain gray matter using likelihood-free inference, in International Conference on Information Processing in Medical Imaging, Springer, 2021, pp. 191–202.

- [11] S. N. JESPERSEN, C. D. KROENKE, L. ASTERGAARD, J. J. ACKERMAN, AND D. A. YABLONSKIY, Modeling dendrite density from magnetic resonance diffusion measurements, *NeuroImage*, 34 (2007), pp. 1473–1486, <http://www.sciencedirect.com/science/article/pii/S1053811906010950>.
- [12] S. G. JOHNSON, Notes on the convergence of trapezoidal-rule quadrature, 2010.
- [13] D. LE BIHAN, E. BRETON, D. LALLEMAND, P. GRENIER, E. CABANIS, AND M. LAVAL-JEANTET, MR imaging of intravoxel incoherent motions: application to diffusion and perfusion in neurologic disorders., *Radiology*, 161 (1986), pp. 401–407, <http://radiology.rsna.org/content/161/2/401.abstract>.
- [14] J.-R. LI, D. CALHOUN, C. POUPON, AND D. L. BIHAN, Numerical simulation of diffusion mri signals using an adaptive time-stepping method, *Physics in Medicine and Biology*, 59 (2014), p. 441, <http://stacks.iop.org/0031-9155/59/i=2/a=441>.
- [15] J.-R. LI AND L. GREENGARD, On the numerical solution of the heat equation i: Fast solvers in free space, *Journal of Computational Physics*, 226 (2007), pp. 1891–1901, <http://www.sciencedirect.com/science/article/B6WHY-4P4NPNB-1/2/38cdafbf0ce301e05c730ed8fc503473>.
- [16] J.-R. LI AND L. GREENGARD, High order accurate methods for the evaluation of layer heat potentials, *SIAM J. Sci. Comput.*, 31 (2009), pp. 3847–3860, <https://doi.org/10.1137/080732389>.
- [17] J.-R. LI, V.-D. NGUYEN, T. N. TRAN, J. VALDMAN, C.-B. TRANG, K. V. NGUYEN, D. T. S. VU, H. A. TRAN, H. T. A. TRAN, AND T. M. P. NGUYEN, Spinductor: A matlab toolbox for diffusion mri simulation, *NeuroImage*, 202 (2019), p. 116120, <https://doi.org/https://doi.org/10.1016/j.neuroimage.2019.116120>, <http://www.sciencedirect.com/science/article/pii/S1053811919307116>.
- [18] J.-R. LI, T. N. TRAN, AND V.-D. NGUYEN, Practical computation of the diffusion mri signal of realistic neurons based on laplace eigenfunctions, *NMR in Biomedicine*, 33 (2020), p. e4353.
- [19] V. MENON, G. GUILLERMO, M. A. PINSK, V.-D. NGUYEN, J.-R. LI, W. CAI, AND D. WASSERMANN, Quantitative modeling links in vivo microstructural and macrofunctional organization of human and macaque insular cortex, and predicts cognitive control abilities, *bioRxiv*, (2019), <https://doi.org/10.1101/662601>, <https://www.biorxiv.org/content/early/2019/06/06/662601>, <https://arxiv.org/abs/https://www.biorxiv.org/content/early/2019/06/06/662601.full.pdf>.
- [20] M. MERcredi AND M. MARTIN, Toward faster inference of micron-scale axon diameters using monte carlo simulations, *Magnetic Resonance Materials in Physics, Biology and Medicine*, 31 (2018), pp. 511–530, <https://doi.org/10.1007/s10334-018-0680-1>, <https://doi.org/10.1007/s10334-018-0680-1>.
- [21] D. V. NGUYEN, J.-R. LI, D. GREBENKOV, AND D. LE BIHAN, A finite elements method to solve the Bloch-Torrey equation applied to diffusion magnetic resonance imaging, *Journal of Computational Physics*, 263 (2014), pp. 283–302, <http://www.sciencedirect.com/science/article/pii/S0021999114000308>.
- [22] K. V. NGUYEN, E. H. GARZON, AND J. VALETTE, Efficient gpu-based monte-carlo simulation of diffusion in real astrocytes reconstructed from confocal microscopy, *Journal of Magnetic Resonance*, (2018), <https://doi.org/10.1016/j.jmr.2018.09.013>, <http://www.sciencedirect.com/science/article/pii/S1090780718302386>.
- [23] V. D. NGUYEN, A fenics-hpc framework for multi-compartment bloch-torrey models, in *EC-COMAS Congress 2016*, vol. 1, 2016, pp. 105–119.
- [24] V.-D. NGUYEN, J. JANSSON, J. HOFFMAN, AND J.-R. LI, A partition of unity finite element method for computational diffusion mri, *Journal of Computational Physics*, (2018), <https://doi.org/10.1016/j.jcp.2018.08.039>, <http://www.sciencedirect.com/science/article/pii/S0021999118305709>.
- [25] V.-D. NGUYEN, J. JANSSON, H. T. A. TRAN, J. HOFFMAN, AND J.-R. LI, Diffusion mri simulation in thin-layer and thin-tube media using a discretization on manifolds, *Journal of Magnetic Resonance*, 299 (2019), pp. 176 – 187, <https://doi.org/https://doi.org/10.1016/j.jmr.2019.01.002>, <http://www.sciencedirect.com/science/article/pii/S1090780719300023>.
- [26] V.-D. NGUYEN, M. LEONI, T. DANCHEVA, J. JANSSON, J. HOFFMAN, D. WASSERMANN, AND J.-R. LI, Portable simulation framework for diffusion mri, *Journal of Magnetic Resonance*, 309 (2019), p. 106611, <https://doi.org/https://doi.org/10.1016/j.jmr.2019.106611>, <http://www.sciencedirect.com/science/article/pii/S1090780719302502>.
- [27] D. S. NOVIKOV, E. FIEREMANS, S. N. JESPERSEN, AND V. G. KISELEV, Quantifying brain microstructure with diffusion MRI: Theory and parameter estimation, *NMR in Biomedicine*, 32 (2019), p. e3998, <https://doi.org/10.1002/nbm.3998>, <https://onlinelibrary.wiley.com/doi/abs/10.1002/nbm.3998>.

- [28] M. PALOMBO, A. IANUS, M. GUERRERI, D. NUNES, D. C. ALEXANDER, N. SHEMESH, AND H. ZHANG, Sandi: a compartment-based model for non-invasive apparent soma and neurite imaging by diffusion mri, *NeuroImage*, (2020), p. 116835.
- [29] M. PALOMBO, C. LIGNEUL, AND J. VALETTE, Modeling diffusion of intracellular metabolites in the mouse brain up to very high diffusion-weight, *Magnetic Resonance in Medicine*, 77 (2017), pp. 343–350, <https://doi.org/10.1002/mrm.26548>.
- [30] E. PANAGIOTAKI, T. SCHNEIDER, B. SIOW, M. G. HALL, M. F. LYTHGOE, AND D. C. ALEXANDER, Compartment models of the diffusion MR signal in brain white matter: A taxonomy and comparison, *NeuroImage*, 59 (2012), pp. 2241–2254, <http://www.sciencedirect.com/science/article/pii/S1053811911011566>.
- [31] G. RENSONNET, B. SCHERRER, S. K. WARFIELD, B. MACQ, AND M. TAQUET, Assessing the validity of the approximation of diffusion-weighted-mri signals from crossing fascicles by sums of signals from single fascicles, *Magnetic Resonance in Medicine*, 79 (2018), pp. 2332–2345, <https://doi.org/10.1002/mrm.26832>, <https://onlinelibrary.wiley.com/doi/abs/10.1002/mrm.26832>, <https://arxiv.org/abs/https://onlinelibrary.wiley.com/doi/pdf/10.1002/mrm.26832>.
- [32] E. O. STEJSKAL AND J. E. TANNER, Spin diffusion measurements: Spin echoes in the presence of a time-dependent field gradient, *The Journal of Chemical Physics*, 42 (1965), pp. 288–292, <https://doi.org/10.1063/1.1695690>.
- [33] D. VAN NGUYEN, D. GREBENKOV, D. LE BIHAN, AND J.-R. LI, Numerical study of a cylinder model of the diffusion mri signal for neuronal dendrite trees, *Journal of Magnetic Resonance*, 252 (2015), pp. 103–113.
- [34] J. VERAART, D. NUNES, U. RUDRAPATNA, E. FIEREMANS, D. K. JONES, D. S. NOVIKOV, AND N. SHEMESH, Noninvasive quantification of axon radii using diffusion mri, *Elife*, 9 (2020), p. e49855.
- [35] A. VRETBLAD, Fourier analysis and its applications, vol. 223, Springer Science & Business Media, 2003.
- [36] D. WASSERMANN, D. V. NGUYEN, G. GALLARDO, J.-R. LI, W. CAI, AND V. MENON, Sensing Von Economo Neurons in the Insula with Multi-shell Diffusion MRI. International Society for Magnetic Resonance in Medicine, 2018, <https://hal.inria.fr/hal-01807704>. Poster.
- [37] A. ZAIMI, M. WABARTHA, V. HERMAN, P.-L. ANTONSANTI, C. S. PERONE, AND J. COHEN-ADAD, AxonDeepSeg: automatic axon and myelin segmentation from microscopy data using convolutional neural networks, *Scientific Reports*, 8 (2018), p. 3816, <https://doi.org/10.1038/s41598-018-22181-4>, <https://www.nature.com/articles/s41598-018-22181-4> (accessed 2022-04-22). Number: 1 Publisher: Nature Publishing Group.
- [38] H. ZHANG, P. L. HUBBARD, G. J. PARKER, AND D. C. ALEXANDER, Axon diameter mapping in the presence of orientation dispersion with diffusion mri, *NeuroImage*, 56 (2011), pp. 1301–1315, <http://www.sciencedirect.com/science/article/pii/S1053811911001376>.